UCRL--98439

DE88 008034

A HIGH-DENSITY, HIGH-TEMPERATURE MIXTURE MODEL

Francis H. Ree
Lawrence Livermore National Laboratory
University of California
Livermore, CA 94550

This paper was prepared for the proceedings of the NATO Conference on
Simple Molecular Systems at Very High Density
Les Houches, France
March 28 – April 6, 1988

March 1988

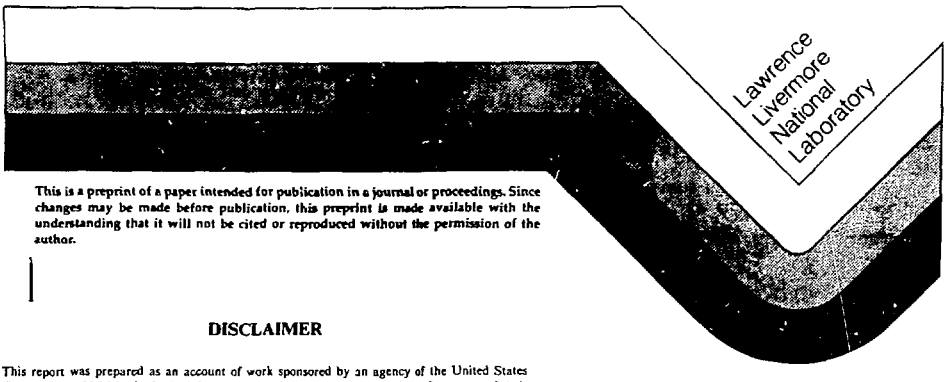

A HIGH-DENSITY, HIGH-TEMPERATURE MIXTURE MODEL

Francis H. Ree

Lawrence Livermore National Laboratory
Livermore, CA 94550 USA

INTRODUCTION

Some of the interesting changes that occur in nature contain mixtures at high pressures and high temperatures. They may involve phase changes and chemical reactions with many chemical species. This particular sub-branch of physics and chemistry has been richly supported by experimental data, but poorly by first-principles theory. Fortunately, for simple systems or complex molecular mixtures at high temperatures, it is possible to develop a reliable statistical mechanical model based on molecular physics, an accurate theory of fluids, and the thermodynamic equations governing mulitphase chemical equilibria.

This paper describes such a mixture model. There are other mixture theories[1] that are more elaborate than the one described in this paper; however, they are either impractical to use (for multicomponent systems, nonspherical forces, many-body forces, etc.) or less accurate at high pressures. The present model is mostly designed for multicomponent systems and is useful for high pressure and high temperature applications. Several recent experimental and theoretical advances aided us in building the mixture model.

1. Experimental shock wave[2,3] and static compression[3] data of many simple molecular species.

2. The availability of the diamond-anvil cell technology for studying a supercritical fluid-fluid phase separation.[4]

3. Reproduction of the experimentally measured data by a priori statistical mechanical methods.[5]

4. A theoretical foundation for making a spherical approximation for nonspherical molecular interactions at high temperatures.[6]

5. Construction of a reliable mixture model by using computer simulations.[7]

6. Development of a sophisticated computer code to solve complex multiphase chemical equilibrium problems.[8]

We will first describe the physical basis and theoretical tools needed for building the mixture model. We then apply the mixture model to binary and ternary mixtures, and to more complex mixtures which are important in understanding the detonation behavior of condensed explosives and the possible states of a planetary interior.

INTERMOLECULAR POTENTIALS

Quantum Mechanical Potentials

A reliable mixture model must give the equation-of-state (EOS) properties of each chemical species in the mixture. This in turn requires information about the intermolecular potential of each chemical species. The most rigorous way of getting this information is to do quantum mechanical calculations. Ideally, we could carry out such calculations for any cluster of molecules, but in practice such calculations become unwieldy for all but the simple molecules.

The hydrogen molecule, with only two electrons, comes very close to the ideal simple molecule. The nitrogen with 14 electrons, has much more complicated electronic interactions. However, in a high-pressure or high-temperature environment, only the strongest forces must be specified accurately, and we can tolerate approximations to the weaker forces. We can obtain a reasonably reliable calculations of the quantum mechanical potential for nitrogen molecules by using the self-consistent field (SCF) method.

Figure 1 compares SCF intermolecular potentials of two H_2[9] and two N_2[10] molecules at four different molecular orientations. For hydrogen, each of the orientations gives the same curve (indicating a highly isotropic nature of the interaction), but for nitrogen, the curves are far apart. At an intermolecular spacing of 2.9 A (about that of the highest shock compression achieved in Ref. 12a from an initially unshocked liquid state), the difference in energy between the X and L geometries (defined in Fig. 1) is about 200 times larger for nitrogen than for hydrogen.

Spherical Potentials for Like-Pair Interactions

The *ab initio* quantum mechanical potentials described above are cumbersome, and we must use simpler potentials (with the same physical features) for mixture calculations. Fortunately, at high temperatures molecules can rotate more easily and such orientational ordering as hydrogen bonding in water can be at least partly broken up. In many dynamic experiments, the compression is still relatively low and the temperature is high enough so that the repulsive force appears to be independent of orientation, even for a highly nonspherical molecule such as N_2. Hence, we need not complicate the expression by explicitly allowing for nonsphericity. A theoretical justification of the spherical approximation has been provided by Shaw, Johnson, and Holian[6a] and Lebowitz and Percus.[6b] They showed that the fluid EOS of a system interacting with a nonspherical potential $V(\underline{r},\omega_1,\omega_2)$ can be approximated by those of a fluid with a spherical potential $V(r)$ equal to the angular median of $V(\underline{r},\omega_1,\omega_2)$.

For a high-pressure and high-temperature application, a spherical potential must be able to describe three essential characteristics: the range of interaction, the depth-of-attraction, and the stiffness of the repulsion. The simplest physically realistic potential which satisfies the above requirement is an exponential-6 (exp-6) potential,

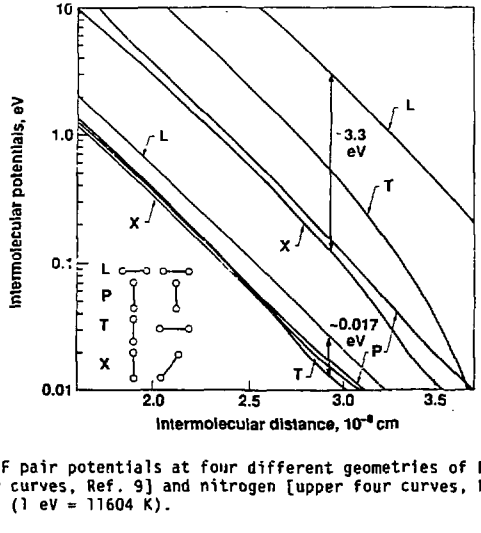

Fig. 1. SCF pair potentials at four different geometries of hydrogen [lower four curves, Ref. 9] and nitrogen [upper four curves, Ref. 10] molecules. (1 eV = 11604 K).

$$V(r) = \frac{\epsilon}{\alpha - 6} \left[6\exp[\alpha(1 - r/r^*)] - \alpha(r^*/r)^6\right], \qquad (1)$$

where parameters ϵ, r^*, and α characterize the depth of the attraction, the magnitude of the repulsive core, and the slope of the exponential repulsion. The above choice of the three-parameter potential, rather than a two-parameter potential, such as the more popular Lennard-Jones (LJ) potential,

$$V(r) = 4\epsilon[(\sigma/r)^{12} - (\sigma/r)^6], \qquad (2)$$

is reasonable here because both quantum mechanical ab initio calculations and analyses of experimental data on simple molecular systems have shown that the intermolecular repulsion must be of an exponential character.

Within a family of exponential potentials, it is convenient to further classify the potential according to its nature of molecular interactions:

Class 1: Potentials that obey the corresponding-states law.
Class 2: Potentials that have a strong electrostatic attraction.
Class 3: Potentials in which many-body interactions are important.

Class 1 Potentials. For molecules such as rare gases, O_2, N_2, CH_4, CO, and CO_2, we have found that $\alpha = 13$ (or a value very close to 13) and that the parameters ϵ and r^* may be fixed by means of the corresponding-states scaling relation.[5] The corresponding-states scaling requires that the parameters r^* and ϵ for the species of interest are derived from the corresponding parameters r_a^* and ϵ_a of argon and critical volumes V_c and temperatures T_c, i.e.,

$$\epsilon/\epsilon_a = T_c/T_{ac}, \qquad (3a)$$

$$r^*/r_a^* = (V_c/Vac)^{1/3}, \qquad (3b)$$

Figure 2 compares experimental shock pressure-density data for nitrogen and carbon dioxide with our theoretical calculations using the statistical mechanical theory developed by Ross.[11] Our calculated EOS agree well with experimental data for CO_2 to all pressures and also for N_2 to about 40 GPa. At higher pressures the experimental shock pressures "softens", (indicating the N_2 fluid becomes easier to compress), possibly because of the pressure- and temperature-induced dissociation of N_2 molecules. Extensive experimental and theoretical work has been done recently on this subject.[12-15]

Class 2 Potentials. For molecules (such as H_2O, NH_3, and HF) with a strong tendency to form hydrogen-bonds, the corresponding-states scaling relation is not applicable. In this case we define the ϵ parameter to be temperature (T) dependent;

$$\epsilon = \bar{\epsilon}(1 + \zeta/T), \qquad (4)$$

where ζ/T accounts for an effective dipole contribution. At temperatures below ζ (about 1000 K for water), the dipole term in ϵ dominates and V(r), at large r, reduces to the Keesom formula, i.e., $V(r) = \text{const}/(Tr^6)$. We can determine ζ either by a quantum-mechanical method[16] or by fitting the Hugoniot data.[17]

Figure 2 compares experimental Hugoniot data for water with the corresponding theoretical calculation. The Hugoniot calculated with temperature-dependent ϵ is in good agreement with the experimental data, even reproducing the ramped "toe" of the curve at low temperatures, while the one (dotted line) calculated without ζ/T term does not agree as well.

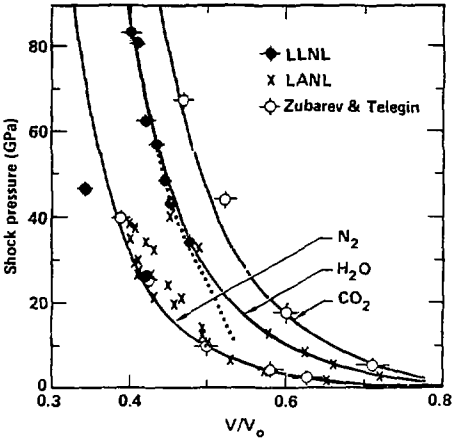

Fig. 2. Comparison of experimental and theoretical Hugoniots of N_2, CO_2, and H_2O. (References on the experimental data are given in Ref. 37.)

Class 3 Potentials. The type of the nonadditive force, relevant to a high-pressure condition is not a triple-dipole ("Axilrod-Teller") interaction which is present at large intermolecular separations, but the type which occurs at short distances as a direct consequence of the Pauli principle. The Pauli principle requires the charge cloud of two molecules to be altered in the presence of a third molecule. In principle, if sufficiently compressed, the EOS of all materials should contain the many-body effect. In practice, however, the EOS of hydrogen is most sensitive to the many-body effect.

To demonstrate this, we used the configuration interaction (CI) calculations for the isosceles geometry of three H_2 molecules.[18] Figure 3 shows the ratio of the triplet potential to pair potential energies for H_2 molecules. At the intermolecular separation of 3.5 Å, the triplet contributions range from -15% for an equilateral geometry to +2% for a linear geometry. In condensed phases there are many equilateral geometries. Thus, the additivity assumption becomes quite poor within the repulsive region of the pair potential. It means that all empirically derived H_2-H_2 potentials in condensed phases are, in fact, "effective" pair potentials with a significant many-body contribution.

In Fig. 4, we compare the ab initio CI and SCF potentials with several such effective potentials: the Silvera-Goldman (SG),[19] Young-Ross (YR), and exp-6 potentials.[20] We note that the YR and exp-6 potentials are nearly identical and softer than the SG potential. The softening for the former two is required to reproduce the shock wave data.[21] This softness may be accommodated in the exp-6 potential by reducing α to 11.1 from 13 for the Class 1 case.

There is a simple physical explanation for the large many-body effect exhibited by the H_2 molecules. They have only two electrons,

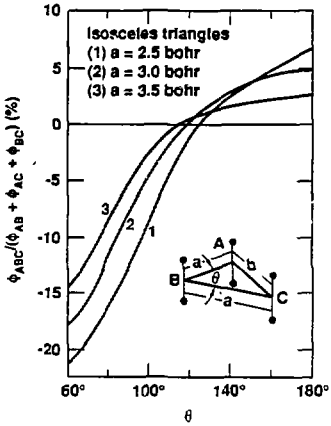

Fig. 3. Ratios (%) of the triplet- to-pair potentials for three H_2 molecules with their axes in parallel orientation.

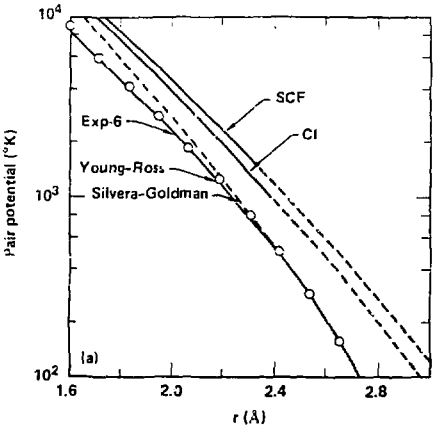

Fig. 4. The effective and the ab initio pair potentials of H_2 molecules (Ref. 20).

but their size is large. Therefore, the electrons are loosely bound to nuclei (i.e, easily polarized) and easily change their charge density when we place the second H_2 molecule nearby. This is the cause for an unusually soft intermolecular repulsion between molecules. Similarly, the placement of the third H_2 molecule alters the charge cloud of a two-H_2 cluster, thereby contributing to the significant three-body potential.

Table I summarizes the exp-6 parameters for many chemical species useful for practical calculations. Because of the three-parameter limitation of the exp-6 potential, these parameters are sometimes useful within a limited range of pressure.

Unlike Pair Potentials

Determining intermolecular potentials for like-pair molecules (i=j) is relatively simple since shock wave data are available for many chemical species of interest. The problem becomes formidable for unlike-pair interactions (e.g., N_2-H_2O), where there are no shock data and potentials derived from gas-phase data are often not reliable in condensed phase problems, condensed-phase interactions being affected by the polarizability of a molecule in the presence of its neighbors. Yet we need information on unlike-pair interaction to model mixtures.

In our model we use the following combination rule:

$$r^*_{ij} = \tfrac{1}{2}\kappa_{ij}(r^*_{ii} + r^*_{jj}), \tag{5a}$$

$$\epsilon_{ij} = k_{ij}\sqrt{\epsilon_{ii}\epsilon_{jj}}, \tag{5b}$$

$$\alpha_{ij} = m_{ij}\sqrt{\alpha_{ii}\alpha_{jj}}, \tag{5c}$$

Table I. Parameters of exponential-6 potentials for chemical species.[a]

Species	ε/k (K)	r*(Å)	α	ζ
Ar	122.0	3.85	13.	0
He	10.8	2.9673	13.1	0
H_2	36.4	3.43	11.1	0
N_2	101.9	4.09	13	0
O_2	125.0	3.84	13	0
CO	108.3	4.12	13	0
CO_2	245.6	4.17	13	0
CH_4	154.1	4.22	13	0
NO	112.9	3.97	13	0
H_2O	356.0	3.06	13	996.8
NH_3	474.0	3.44	13	441.0
C_2H_2	249.4	4.50	13	0
C_2H_6	246.8	4.86	13	0
C_3H_8	298.9	5.43	13	0
CH_3OH	414.6	4.92	13	0
N_2O	250.1	4.26	13	0
NO_2	348.4	4.27	13	0

[a] Parameters for the first eleven species are from Refs 5, 30, and 37. See references quoted therein for original papers. Parameters for the remaining species are derived using the corresponding states scaling relation (Ref. 5).

where κ_{ij}, ξ_{ij}, and m_{ij} are unity (i.e., the Lorentz-Berthelot rule) for most cases. They can be adjusted to agree with experimental mixture data if they are available. Typical uncertainties of the Lorentz-Berthelot rule are about 5%.

ONE-COMPONENT EOS

The mixture model should give accurate EOS data for pure phases of individual components in the mixture. Also, it should permit rapid evaluations of thermodynamic properties. There are two such models, both based on one-component statistical mechanical theories.

We first describe Ross's soft-sphere variational procedure,[11] which is an extension of the hard-sphere variational theories of Mansoori and Canfield, and Rasaiah and Stell. Briefly, the Helmholtz free energy A is expressed as the sum of the free energies of different degrees of freedom,

$$A = A_t + A_r + A_v + A_e + A_{pE}, \tag{6}$$

where subscripts t, r, v, and e denote the contributions by the translational, rotational, vibrational, and electronic degrees of freedom. The free energies of these degrees of freedom are assumed to be those of an isolated molecule. The electronic excitation is usually negligible within the temperature range of 4000 K or lower. The potential energy contribution A_{pE} is obtained by minimizing the right-hand side of

$$A_{pE} = A_{HS} + F(\eta)NkT + (\rho N/2) \int d\underline{r}\, V(r) g_{HS}(r,\eta) + A_{qm} \tag{7}$$

with respect to the hard-sphere diameter d. This appears in the

"packing" fraction $\eta = \pi d^3\rho/6$ (ρ = the number density) in Eq. (7). The quantities $A_{HS}(\eta)$ and $g_{HS}(r,\eta)$ represent the hard-sphere excess free energy and the hard-sphere radial distribution function. The factor $F(\eta) = -(\eta^4/2 + \eta^2 + \eta/2)$ makes the computed thermodynamic quantities agree with the corresponding Monte Carlo data for a different class of potentials. A_{qm} is the first order quantum correction in the Wigner-Kirkwood expansion:

$$A_{qm} = (h^2\rho N/96\pi^2 mkT) \int d\underline{r}\; g_{HS}(r,\eta)\nabla^2 V(r). \tag{8}$$

The potential V(r) can be either temperature independent or temperature dependent, as in Eq. (4). The pressure P and internal energy E are calculated by taking the appropriate numerical derivatives of Eq. (6). We will exclusively use the above variational theory in later sections of this paper.

We describe next an alternative to the above approach, a perturbation method,[22] which will be equally useful in future applications. It starts from van der Waals's idea that V(r) may be broken up into a strong, short-range repulsive reference potential $V_0(r)$ and the remaining mainly long-range perturbation $V_1(r)$:

$$V(r) = V_0(r) + V_1(r), \tag{9}$$

$$\begin{aligned} V_0(r) &= V(r) - F(r), && \text{if } r \le \lambda, \\ &= 0, && \text{if } r \ge \lambda, \end{aligned} \tag{10}$$

$$\begin{aligned} V_1(r) &= F(r), && \text{if } r \le \lambda, \\ &= V(r), && \text{if } r \ge \lambda, \end{aligned} \tag{11}$$

where

$$F(r) = V(\lambda) - [dV(r)/dr]_{r=\lambda}\,(\lambda - r), \tag{12}$$

$$\lambda = \sqrt{Z}/\rho^{1/3}. \tag{13}$$

Note that Eq. (4) represents the nearest-neighbor distance of a close-packed fcc or hcp lattice, and that Eqs. (10) and (11) reduce to the theory of Weeks, Chandler, and Andersen (WCA) if F(r) and λ are chosen constant. The perturbation theory expands A_{PE} in a series involving $V_1(r)$. The final result is given by

$$A_{PE} = A_{HS} + (\rho N/2) \int d\underline{r}\; V_1(r) g_{HS}(r,\eta), \tag{14}$$

where η is given by solving for the root of

$$\int d\underline{r}\; \{\exp[-V_0(r)/kT] - \exp[-V_{HS}(r)/kT]\} \exp[V_{HS}(r)/kT]\; g_{HS}(r,\eta) = 0. \tag{15}$$

Characteristic features of the perturbation theory are: (1) its ability to handle both fluids and solids and (2) the use of $V_0(r)$ whose range λ shrinks with density. Table IIA shows a comparison of PV/NkT for an exp-6 potential. Calculating a melting transition provides another test of the new theory. This is done in Table IIB for a LJ system. It also reveals an excellent agreement over a wide density and temperature range.

Table IIA. Comparison of PV/NkT for the exp-6 system at $kT/\epsilon = 20$. PT = the perturbation theory (Ref. 22), Ross = the Ross theory (Ref. 10).

	PV/NkT					
	Fluid			Solid		
$\rho(r^*)^3/\sqrt{2}$	Exact[a]	PT	Ross	$\rho(r^*)^3/\sqrt{2}$	Exact[a]	PT
0.9	3.27	3.27	3.32	2.308	20.28	0.28
1.0	3.81	3.80	3.87	2.76	30.88	0.38
1.25	5.52	5.55	5.68			
1.50	8.07	8.04	8.19			
1.75	11.34	11.37	11.54			
2.0	15.55	15.66	15.84			
2.05	16.58	16.65	16.80			

[a] Monte Carlo values. See Ref. 22 for their original sources.

Table IIB. Melting lines of the LJ system obtained by the computer simulations[a] and the perturbation theory (PT) (Ref. 22).

	Freezing density ($\rho_f\sigma^3$)		Melting density ($\rho_s\sigma^3$)		Pressure ($P\sigma^3/\epsilon$)	
kT/ϵ	Exact	PT	Exact	PT	Exact	PT
0.75	0.875	0.865	0.973	0.958	0.67	0.65
1.35	0.964	0.986	1.053	1.058	9.00	9.60
2.74	1.113	1.144	1.179	1.210	32.2	36.8
5	1.279	1.305	1.349	1.371	86	93
10	1.500	1.526	1.572	1.599	231	247
20	1.765	1.793	1.843	1.874	590	627
50	2.200	2.231	2.291	2.327	1970	2070

[a] J.-P. Hansen and L. Verlet, Phys. Rev. 184:151 (1969); J.-P. Hansen, Phys. Rev. A 2:221 (1970).

MIXTURE EOS

The theoretical and experimental work we have discussed up to this point is a necessary preliminary to the description of mixture EOS. To calculate anything about mixtures involving many species, we must, in addition to sphericity and effective pair potentials, employ another simplifying assumption. We describe below such an approximation for both two- and three- parameter potentials.

One-Fluid Van der Waals Model

The one-fluid van der Waals (vdWlf) model is a widely used mixture theory that is appropriate for molecules interacting with two-parameter potentials. It is applicable only if the mixture potential has the form

$$V(r_{ij}) = \epsilon_{ij} f(r/r^*_{ij}). \qquad (16)$$

In these equations r^*_{ij} and ϵ_{ij} denote respectively the range of interaction and the depth of attraction for the chemical species i and j. In the vdWlf model all molecules in the mixture are assumed to be identical and to interact by an "effective" one-component potential with the same functional form as the original potential for individual pairs.

For the effective one-component potential, r* and ϵ parameters are chosen to depend on $\{x_i\}$ in the following manner:

$$(r^*)^3 = \sum_{i,j} x_i x_j (r^*_{ij})^3, \tag{17}$$

$$\epsilon = \sum_{i,j} x_i x_j \epsilon_{ij} (r^*_{ij})^3 \; / \; (r^*)^3, \tag{18}$$

where x_i is the mole fraction $(n_i/\sum_j n_j)$ of chemical species i and summations extend over all chemical species (with mole numbers $\{n_i\}$) which are present in a phase of interest. Note that the effective ϵ and r^* parameters are composite or weighted averages specified in terms of the concentrations. Since in this model every molecule interacts with the same potential as every other molecule, we can extend the one-component EOS systems discussed earlier to mixtures.

Henderson and Leonard,[23] using computer simulation data for the LJ mixtures, have shown that the vdWlf model gives excess thermodynamic properties that are either comparable to or often superior to calculations based on more elaborate theories. The vdWlf model has been cast in a rigorous theoretical framework by Smith.[24] Henderson and Leonard have obtained Eqs. (17) and (18), assuming that the the radial distribution functions of both the mixture and the effective one-component fluid have the same form, i.e.,

$$g_{ij}(r) = G(r/r^*_{ij}), \tag{19}$$

$$g(r) = G(r/r^*). \tag{20}$$

The second way of obtaining the vdWlf model is that of MacGowan, Lebowitz, and Waisman,[25] who demand that both the mixture and the vdWlf model give the same compressibility:

$$kT(\partial\rho/\partial P)_T = 1 + \rho \sum_{i,j} x_i x_j \int d\underline{r} \, [g_{ij}(r) - 1] \; . \tag{21}$$

If we substitute Eqs. (19) and (20) into Eq. (21) and equate the two, we obtain Eq. (18).

The above results and the fact that one-component statistical mechanical calculations are generally simpler than full mixture calculations provide a reasonable justification for using the vdWlf model in problems that would be otherwise computationally impractical.[26]

Improved Van der Waals One-Fluid Model

Real molecular interactions are more complex than the expression employed in the vdWlf model. Thus, the applicable range of the vdWlf model is reduced to a limited density and temperature interval where major contributions to thermodynamic properties come from that portion of the potential approximated by the two-parameter form. This limitation makes the vdWlf model less useful in problems involving extreme temperatures and pressures. For example, a computation of detonation properties of condensed explosives and a prediction of the interior

compositions of Jupiter and Saturn require a consideration of temperatures to 5000-10000 K and pressures to 50-200 GPa. Here a large range of the intermolecular repulsion r^* and, therefore, stiffness α play a dominant role. Unlike the vdWlf assumption, however, the stiffness of the repulsion varies from species to species. Thus, it is necessary to derive a proper formula for the α parameter that is analogous to r^* and ϵ in Eqs. (17) and (18).

In order to develop such a formula, we first carried out two-component Monte Carlo calculations for H_2-He mixtures using exp-6 potentials for individual pairs.[7] Next, these results are compared against similar Monte Carlo calculations for several effective one-component systems to find out which of these systems can best approximate the two-component system. In these tests we kept the same r^* and ϵ of the one-component systems in Eqs. (17) and (18) but varied α by expressing them as a sum of products of α_{ij}'s, r^*_{ij}'s, ϵ_{ij}'s, and x_i's; for example,

$$\alpha = \sum_{i,j} x_i x_j \alpha_{ij} \epsilon_{ij} (r^*_{ij})^3 \; / \; \epsilon (r^*)^3, \tag{22}$$

$$\alpha = \sum_{i,j} x_i x_j \alpha_{ij}, \tag{23}$$

$$\alpha = \sum_{i,j} x_i x_j \alpha_{ij} \epsilon_{ij} \; / \; \epsilon, \tag{24}$$

In Table III we compare the resulting pressure data with the corresponding two-component results for 108 H_2 molecules and 108 He atoms. We note that, compared to Eqs. (23) and (24), Eq. (22) gives clearly superior results. Differences between the results based on Eq. (22) and the two-component results are 2.3% in P and 1.25 % for the excess energy. Table IV compares the results from Eq. (22) with the two-component calculations over a wider range of T and V for an equimolar mixture. We note that the agreement is nearly perfect within the pressure range below 3 GPa, falling slightly (1%-3%) below the two-component results at higher T ($\geq$ 1000 K). These differences are slightly larger than statistical errors in the Monte Carlo data. Errors of this magnitude are also present in the conventional vdWlf model. Therefore, the improved vdWlf model probably comes close to an optimum form.

Recently, MacGowan et al.[25] gave another expression for α,

$$\alpha = \sum_{i,j} x_i x_j \alpha_{ij} (\alpha_{ij}-6)(\alpha_{ij}-7) \epsilon_{ij} (r^*_{ij})^3 \; / \; \epsilon (r^*)^3 (\alpha-6)(\alpha-7). \tag{25}$$

The above formula is obtained by using the first two non-vanishing terms in the Taylor expansion of $V(r_{ij})$ about r^*_{ij} in the energy equation and by demanding that both the mixture and effective one-component results give the same energy. They showed that, since the α_{ij}'s, in practice, are all in the range 11-14, both Eqs. (22) and (25) give similar results.

It is known that the conventional vdWlf model becomes less reliable if mixture particles have substantially different repulsive cores. The size of the repulsive cores in the improved vdWlf model is determined by r^* and α. In this respect, it is worth noting that the H_2-H_2 and He-He potentials used in Table IV differ substantially not only in the stiffness α but also in the range and magnitude of the interactions, i.e., $\epsilon_{H_2H_2}/\epsilon_{HeHe} = 3.45$ and $(r^*_{H_2H_2}/r^*_{HeHe})^3 = 1.6$. The H2-H2 repulsion, despite its longer range (r^*), is much softer than the He-He repulsion. This probably contributed to the good agreement obtained in Table IV. From these calculations, we can conclude that Eq. (22) for α, coupled

Table III. A Monte Carlo test of three effective one-component α's against the two-component data for an equimolar mixture of H_2 and He at 4000 K and 8 cm^3/mole (Ref. 7).[a]

Formula	Pressure (GPa)	Energy (kJ/mol)	α
Two-component	12.43	25.12	- - -
Eq. (22)	12.43	25.12	11.983
Eq. (23)	12.15	24.82	15.525
Eq. (24)	13.59	26.98	11.487

[a] The H_2-H_2, He-He and H_2-He exp-6 parameters: (r^*, ϵ/k, α) = (3.43 Å, 36.4 K, 11.1), (2.97 Å, 10.57 K, 13.6), and (3.37 Å, 15.5 K, 12.7), respectively.

Table IV. The Monte Carlo pressure of an equimolar H_2-He mixture.[a] (Ref. 7)

T (K)	V (cm^3/mol)	Pressure (GPa)	
		Two-Component	One-Component
50	20	0.047	0.048
100	14	0.034	0.034
300	10	1.86	1.86
1000	9	4.51	4.42
4000	8	12.43	12.15
7000	4.5	54.01	52.53

[a] See footnote a in Table III for the exp-6 parameters used here.

with the usual vdWlf model, should be used to compute thermodynamic properties at high pressures, where it is physically less appropriate to use the conventional model.

Quantum Correction for The Effective One-Component Model

To accommodate the quantum correction A_{qm} [Eq. (8)] within the framework of the effective one-component model, we need a proper effective one-component mass m that is analogous to r^*, ϵ, and α described earlier. It is possible to derive such an expression by following the dimensional analysis used by Henderson and Leonard.[23] The resulting expression[27] is

$$1/m = \sum_j (1/m_j) x_i x_j \epsilon_{ij} r^*_{ij} \; / \; \epsilon r^*. \qquad (26)$$

We have computed A_{qm}, P_{qm}, and E_{qm} by the Monte Carlo method using the relations derived by Barker et al.[28] Table V summarizes the calculations performed for both the two-component mixtures (216 H_2 molecules and He atoms) and the effective one-component mixtures [obeying Eqs. (17), (18), (22), and (26)] at three different H_2:He

ratios. The classical and quantum corrections to P and E are separately listed to indicate their relative sizes. The two- and one-component results show that the deviations between the two are small, lying either close to or within statistical errors. This result further substantiates the reliability of the effective one-component formulas for ϵ, r^*, α, and m. Theoretical results in Table V refer to the results based on Ross's theory. They are similarly encouraging. They give the pressures which lie (<3-5%) above the Monte Carlo results. Agreement in E is generally better.

BINARY AND TERNARY MIXTURES - SUPERCRITICAL PHASE SEPARATION

Using the theoretical tools described above, we are in a position to compute $(P,T,\{x_i\})$ boundaries of a phase separation. For this purpose, we use the Gibbs free energy $G(P,T,\{x_i\})$ rather than the Helmholtz free energy A.

For many pure components (x = 1 or 0), their exp-6 parameters are reasonably well known. (See Table I.) In principle, it is possible to determine the unlike-molecular interactions by matching a theoretical solubility boundary to experimental data. We will consider:

(1) Binary nonpolar molecular mixtures
(2) Binary monatomic mixtures
(3) Binary mixtures with polar molecules
(4) Ternary mixtures

Data on fluid phase separations are available for (1) - (3) in the pressure range up to 1 to 8 GPa. The systems of interest are. H_2-He and N_2-CO_2 for (1); He-Xe for (2); H_2O-N_2, H_2O-CO_2 and N_2-CO_2 for (3); and N_2-CO_2-H_2O mixtures for (4).

Table V. Pressure P and excess internal energy E/NkT of H_2-He mixtures at 61.5 K and 15 cm^3/mole.[a] The classical and quantum mechanical contributions are separately listed. (Ref. 7)

			P(MPa)		E/NkT	
		H_2:He	class.	quantum	class.	quantum
Two-component	MC	3:1	212	101	-2.273	1.94
One-component	MC	3:1	213	100	-2.231	1.94
Theory[b]		3:1	222	103	-2.228	2.00
Two-component	MC	1:1	167	74	-1.431	1.35
One-component	MC	1:1	168	58	-1.395	1.25
Theory		1:1	174	68	-1.405	1.32
Two-component	MC	1:3	130	38	-0.814	0.78
One-component	MC	1:3	129	33	-0.801	0.76
Theory		1:3	134	39	-0.809	0.82

[a] Values of the (r^*, ϵ/k, α) parameters for the H_2-He interaction are (3.30 Å, 15.5 K, 13). The pure-component parameters are given in Table I.

[b] Calculations using the Ross theory.

One can study the phase separation in these systems using either a nonreactive method (which does not make use of chemical reactions) or the reactive method (in which the phase separation is treated as a chemical reaction problem). The former gives an accurate phase boundary close to the critical line; however, the method is too complex to apply beyond binary mixtures. On the other hand, since the second approach is designed for a mixture with an arbitrary number of components, it too has a shortcoming in that it uses a mathematical algorithm which is not really designed for computing a phase boundary near the critical line. We will use the first method to compute the phase boundary of H_2-He mixtures, and the second method for studying the other systems.

Determination of A Phase Boundary by A Nonreactive Method

To determine the phase boundary of a binary mixture of species a (mole fraction x) and b (mole fraction 1-x), we fix pressure P and temperature T and solve for a pair of compositions (x' and x'') at which the excess Gibbs free energy

$$\Delta G(P,T,x) = G(P,T,x) - xG(P,T,1) - (1-x)G(P,T,0) \qquad (27)$$

has a common tangent. The procedure requires: we first relate G to the Helmholtz free energy A by a thermodynamic definition, $G = A + PV$, (V = volume), and then evaluate $P(V,T,x)$ and $A(V,T,x)$ over a sufficiently large range of V and x so that the resulting data may be inverted by interpolation to yield $G(P,T,x)$. The only link between the above thermodynamic procedure and theoretical mixture models (described earlier) occurs in the evaluation of $A(V,T,x)$ [Eq. (6)] which in turn requires the information on intermolecular potentials for pure (x= 0 or 1) and mixtures.

Application to H_2-He Mixtures

It is well known that liquids, such as water and oil, do not mix well with each other. Less known is the fact that a similar "demixing" occurs in gas mixtures above their critical temperatures. Since van der Waals first predicted this so-called supercritical phase separation, such phase separations have been found in approximately one hundred binary mixtures. Recent diamond-anvil cell experiments by van den Bergh, Schouten, and Trappeniers[4a] and Loubeyre, Le Toullec, and Pinceaux[4b] show that the fluid phase separation in the H_2-He mixture extends to at least 15 GPa and 400 K. These experiments stand out as the highest pressure experiments on fluid phase separation. At such a high pressure and temperature the molecular interactions are almost totally repulsive. These data and the earlier data obtained by Streett[29] provide us the most complete system for testing a theoretical mixture model at high pressures.

Theoretically, the H_2-He system is important. First, both H_2 and He have small masses. Hence, its EOS should exhibit appreciable quantum corrections, providing a practical check to the effective mass formula, Eq. (27). Second, we have already described how a large many-body effect in H_2 molecules gives rise to the soft-repulsion in the H_2-H_2 effective potential. It is an ideal system to test the mixing rule, Eq. (22), for the stiffness parameter α.

There is a large body of experimental and theoretical information on pure solid and liquid H_2 and He. As a consequence, we now have a reasonably good understanding on the physical behavior of the individual components. The experimentally reported static measurements include the solid and fluid isotherms. Shock wave data are also available for both

H_2 and He. (Reference 27 gives references on experimental works.)

In our work we use the exp-6 parameters for the H_2-H_2 potential which can accurately represent single and double shock data of liquid H_2 and D_2 to 90 GPa or to 7000 K. The same parameters also describe experimental static compression data reasonably well. The exp-6 He-He parameters in Table I are taken from Young et al.'s work.[30] These parameters can accurately reproduce experimental (P,V) and melting-curve data up to 12 GPa.

In contrast, practically no information is available on the exp-6 parameters for the H_2-He interaction in condensed phases. In Fig. 5a the theoretical solubility lines have been matched to Streett's experimental data by choosing $(r^*_{H_2He}, \epsilon_{H_2He}/k, \alpha_{H_2He}) = (3.28\ \text{Å}, 17.3\ \text{K}, 12.54)$. These values are 2.5% above, 13% below, and 4% above the corresponding Lorentz-Berthelot values, respectively. At fixed temperatures the demixing region corresponds to a region in which the pressure and composition lie above the solubility line in Fig. 5(a). Both theoretical and experimental solubility lines agree satisfactorily at $T \geq 61.5$ K. Disagreement below 61.5 K is due to higher-order quantum corrections that were not considered in the calculation. In Fig. 5(a) dash-dotted lines, indicating theoretical freezing lines along the isotherms, are approximated by assuming that the hard-sphere packing fraction η is constant (0.44) along the freezing lines. This empirical rule gives usually reliable melting lines for other potentials. Intersections of the freezing lines and the solubility lines in Fig. 5(a) define the pressures (dashed lines) at which the H_2-rich solid phase coexists in equilibrium with the H_2-rich and He-rich fluid phases. The corresponding experimental data are marked by solid circles.

The above calculation gives information on the exp-6 parameters (r^*, ϵ, α) for the H_2-He interaction. A cursory investigation of the sensitivity of the solubility lines to the variation of these parameters indicates that the solubility lines are most sensitive to the change in $r^*_{H_2He}$ and are least affected by the change in ϵ_{H_2He}. The change of ϵ_{H_2He}/k over 14-17 K, as predicted by various theoretical and experimental studies, did not alter the solubility lines appreciably. While an increase of $r^*_{H_2He}$ by 0.02 Å lowered the pressure of the 100 K solubility line by about 150 MPa at $x_{H_2} = 50\%$, without "tilting" the solubility line in favor of the H_2- or He-rich fluid phase. Similar effects may be produced by increasing α_{H_2He}. In this case, however, the solubility line is lowered more at lower x_{H_2} values.

We have extended the above calculations (≤ 1 GPa) to 7 GPa using the same exp-6 parameters. Figure 5(b) compares the computed phase boundaries at 200 K and 300 K with van den Bergh et al.'s diamond-anvil cell data.[4a] We note that the agreement between the two is satisfactory except near the critical points. It will be possible to match the experimental data by further "fine-tuning" the H_2-He interaction parameters. Near the critical line [loci of the minima of the solubility isotherms in Figs. 5(a) and 5(b)], however, the Gibbs free energies of the two fluid phases are almost equal. Hence, in Fig. 5(b) the computed phase boundaries near the critical points contain some uncertainties. Therefore, the fine-tuning procedure requires a very precise method of evaluating the Gibbs free energy. Figure 6 shows the experimental and theoretical critical lines for the H_2-He system. The agreement between the two is good.

The most significant result of the above study is that the H_2-He system exhibits a supercritical fluid phase separation at the (T,P) range of van der Bergh et al.'s experiment, where the molecular

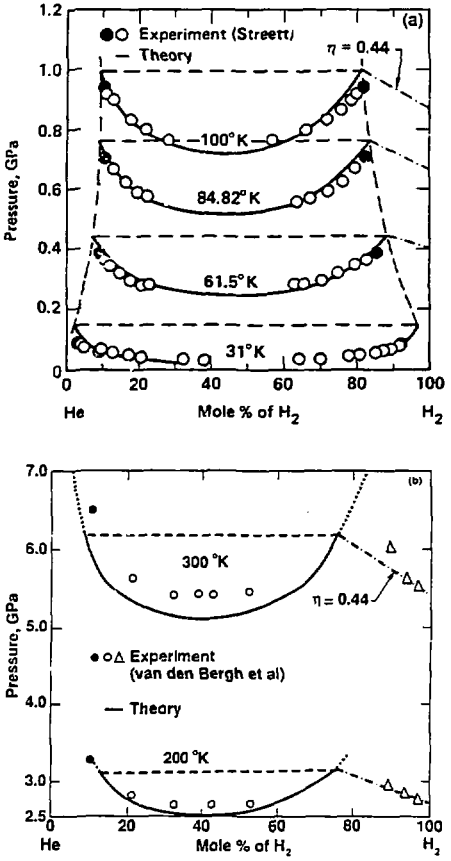

Fig. 5. Solubility lines of the H_2-He system at (a) $P \leq 1$ GPa and (b) $P > 1$ GPa: open circles = experimental data from Refs. 4a and 29; solid lines = theory (Ref. 27). Solid circles and open triangles represent, respectively, the experimental three-phase (two fluids and one solid) and two-phase (single fluid and solid) states. The dashed-dot lines = theoretical melting line based on the assumption $\eta = 0.44$.

interactions are almost totally repulsive. The phase separation may originate from the way molecules with different sizes can pack most efficiently. This is supported by our calculation, but they have been neglected in many available theoretical models. The factor most responsible for the fluid phase separation is the repulsive parameter $r^*_{H_2He}$. In the case of hard-sphere mixtures with the unlike hard-sphere

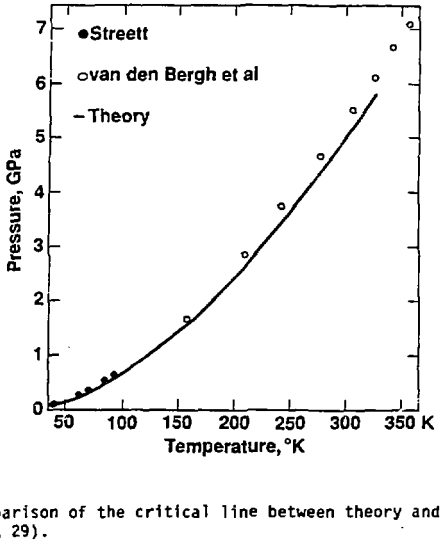

Fig. 6. Comparison of the critical line between theory and experiment (Refs. 4a and 29).

diameter given by

$$d_{ab} = \tfrac{1}{2}(d_{aa} + d_{bb})(1 + \theta), \tag{28}$$

Melnyk and Sanford[31] have made a molecular dynamic simulation and other theoretical calculations. Their results indicate a fluid phase separation only if $\theta > 0$. But the transition occurs in the metastable fluid range if θ is too small or if $\theta = 0$. The latter case has been investigated by Lebowitz and his coworkers[32] and Alder.[33] However, as Lebowitz and Zomick noted, for real fluids at high pressures there is no compelling reason that θ should be zero.

Determination of A Phase Boundary By A Reactive Method

We will describe below an alternative and more general way to compute a phase boundary for a multicomponent mixture. For this purpose, it is convenient to treat a single chemical compound, if it occurs in more than one phase, as different species. Thus, a phase change, for example, is treated as a chemical reaction involving two distinct species.

Briefly, we set up R independent chemical reactions involving species A_j (= 1, 2, ..., ℓ),

$$\nu_{1j}A_1 + \nu_{2j}A_2 + \nu_{3j}A_3 + \ldots + \nu_{\ell j}A_\ell = 0, \tag{29}$$

where j = 1, 2,..., R, and $\{\nu_{ij}\}$ is a set of stoichiometric coefficients (negative signs for reactants and positive signs for products). If we define λ_j (the so-called extent-of-reaction variable) as the fraction of

reaction j that is completed, the total change in the number of mole n_i of species A_i for all reactions is

$$n_i = n_{i0} + \sum_{j=1}^{R} \nu_{ij}\lambda_j, \quad i = 1,2,\ldots,\ell. \tag{30}$$

Initially, all λ_j's are zero; they are unity at the final state.

Since $\{n_i\}$ and $\{\lambda_j\}$ are related by Eq. (30), the Gibbs free energy which is a function of P, T, and $\{n_i\}$ can also be represented as a function of P, T, and $\{\lambda_j\}$. Thus, the minimization of $G(P,T,\{\lambda_j\}))$ at fixed P and T implies

$$\partial G/\partial\lambda_j = \sum_{i=1}^{\ell} \nu_{ij}\mu_i = 0, \quad j = 1,2,\ldots,R. \tag{31}$$

In Eq. (31) $\mu_i = \partial G/\partial n_i$ represents the chemical potential of species i. We compute μ_i from the mixture EOS described in the preceding sections. The resulting expression for μ_i is a complex function of P, T, and $\{n_i\}$, given in Ref. 8.

The above mathematical formulation is programmed into the chemical equilibrium (CHEQ) code. The CHEQ code solves for $\{n_i\}$ using Eqs. (30) and (31) with an additional constraint (the stoichiometric condition), conserving the total number of elements before and after the chemical reactions. We use the resulting G to computes thermodynamic quantities by taking appropriate numerical derivatives of G.

Application to The Xe-He System

Reactions (29) for the supercritical phase separation between a Xe-rich (f1) phase and a He-rich (f2) phase are given by

$$\text{Reaction 1: } Xe(f1) - Xe(f2) = 0, \tag{32a}$$

$$\text{Reaction 2: } He(f1) - He(f2) = 0. \tag{32b}$$

The extents of these reactions are λ_1 and λ_2; hence, Eq. (30) gives the resulting changes in the mole numbers,

$$n(Xe,f1) = n_0(Xe,f1) + \lambda_1, \tag{33a}$$

$$n(Xe,f2) = n_0(Xe,f2) - \lambda_1, \tag{33b}$$

$$n(He,f1) = n_0(He,f1) + \lambda_2, \tag{33c}$$

$$n(He,f2) = n_0(He,f2) - \lambda_2, \tag{33d}$$

The chemical equilibrium conditions Eq. (31) imply

$$\mu(Xe,f1) = \mu(Xe,f2), \tag{34a}$$

$$\mu(He,f1) = \mu(He,f2). \tag{34b}$$

The CHEQ code solves for the solution $\{n_i\}$ which satisfies Eqs. (33) and (34). In Fig. 7 the resulting theoretical solubility lines of the Xe-He system[34] are compared with the experimental data of de Swaan Arons and Diepen's data.[35] The calculations are based on like-pair exp-6 parameters derived from the corresponding-states scaling

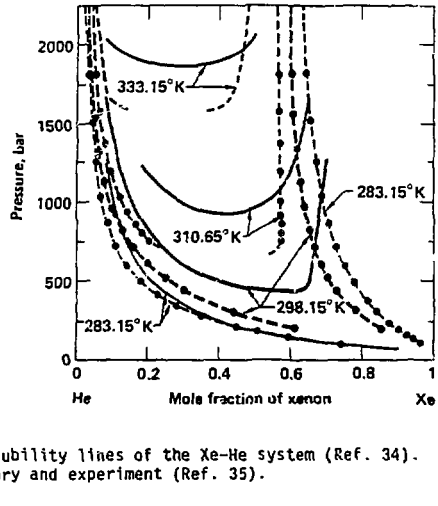

Fig. 7. Solubility lines of the Xe-He system (Ref. 34). Comparison between theory and experiment (Ref. 35).

relations[5] and the unlike-pair ϵ_{ij} values from an empirical rule.[36] Since the main purpose of the calculations was on testing the CHEQ code, no attempt was made to "fine-tune" the exp-6 parameters. Therefore, it is encouraging to see reasonable agreement between theory and experiment. Near the critical region, however, the theoretical results tend to become "stiffer". This unphysical behavior is connected with our use of the free energy expression, Eq. (7), which becomes nonconvex with respect to variation of n_i's.

In this connection, it is worthwhile to briefly mention the procedure for determining the phase separation boundaries by the CHEQ code. We fix T and initial values for $\{n_i\}$. We then start our calculation at a high P, where a mixed-fluid phase has a much lower Gibbs free energy G than that of the homogeneous fluid phase so that the CHEQ code can find the phase boundary without difficulty. We determine the phase boundaries at successively lower pressures until the calculation predicts a homogeneous fluid phase. Because we are using the same analytic G to describe different fluid phases by analytic continuation, the observed homogeneous fluid phase may be thermodynamically metastable or stable. That is, when plotted against the composition, G shows a wiggly shape with its curvature changing from + to - to +. That portion of G having the positive (convex) curvature is thermodynamically stable or metastable, while the negative (nonconvex) curvature represents a thermodynamically unstable region. For complex mixtures for which the CHEQ code is designed, the composition variables are multi-dimensional and there is no simple procedure to solve for $\{n_i\}$. The CHEQ code makes use of the convexity of G. Within or near a fluid phase boundary, this procedure can lead to a local minimum (representing a metastable homogeneous phase). We can mostly avoid such a possibility by repeating the calculation using different initial compositions. If none of them predicts the mixed phase, we consider the (P,T) state to be in a homogeneous fluid phase. Otherwise, it is in the mixed phase region. We have tested the above procedure against calculations using the double-

tangent construction for binary mixtures. The present procedure works for most cases except near the critical point of the solubility isotherms, where the free energy difference is very small and is insensitive to composition.

Fluid Phase Separations in N_2, H_2O, and CO_2 Mixtures

Since N_2, CO_2, and H_2O are major detonation products of HE, we investigated the phase behavior of their mixtures. Figure 8(a) shows that, at (P,T) states relevant to HE detonation, the N_2-H_2O mixture can separate into two fluid phases, one rich in N_2 and the other rich in H_2O.[37] This result implies that a proper description of detonation behavior needs to deal with the supercritical fluid phase separation in the N_2-H_2O system. In contrast, the fluid phase separations in the

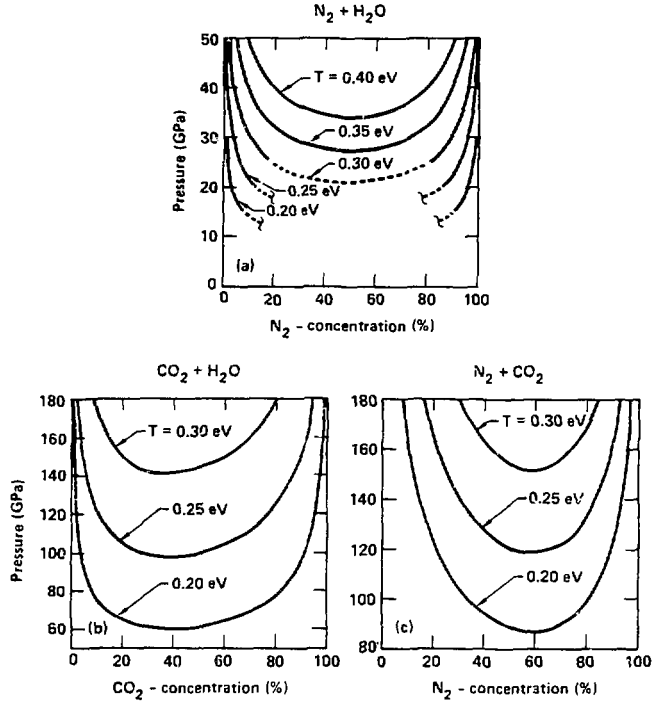

Fig. 8. Theoretical solubility lines of three binary systems (Ref. 37): (a) N_2-H_2O, (b) CO_2-H_2O, and (c) N_2-CO_2. They are based on the like-pair exp-6 parameters in Table I and the unlike-pair parameters: $r^*_{N_2H_2O}$ = 3.575 Å, $r^*_{CO_2H_2O}$ = 3.615 Å, and $r^*_{N_2CO_2}$ = 4.13 Å. Dashed or broken portions of the isotherms are theoretically unreliable portions. See the text.

CO_2-H_2O and N_2-CO_2 systems [Figs. 8(b) and 8(c)] occur at pressures above 60 GPa for the CO_2-H_2O mixture and above 80 GPa for the CO_2-N_2 mixture. These ranges probably lie outside the stability range of the fluid phases for these mixtures. The present procedure works for most cases except near the bottom portions (i.e., P < 25 GPa) of the low-T solubility isotherms, where the free energy difference is very small and is insensitive to composition. Those portions of the solubility isotherms, where the CHEQ code is trapped in the metastable homogeneous phase, are either left out or indicated by dashed lines in Fig. 8.

Experimental data on the N_2-H_2O system[38] and the CO_2-H_2O system[39] are limited below 0.4 GPa and temperatures below 700 K. These data lie well below the temperature range (> 1300 K) where our model [Eqs. (4)] of water is applicable. Nevertheless, the experimental data show a large (T,P) region of incomplete miscibility for the N_2-H_2O system and an equally large region of complete miscibility for the CO_2-H_2O system. This is consistent with the results discussed above.

Figure 9 shows a typical solubility diagram for a ternary system of N_2, CO_2, and H_2O at 33 GPa and 0.35 eV (1 eV = 11604 K), a state near the theoretical Chapman-Jouguet (C-J) point of PBX-9404 (open circle). We note that CO_2 tends to make N_2 more soluble in water, in much the same way that soap makes oil and water more miscible. The shaded area represents the fluid phase separation, otbtained by using Eq. (5) for the unlike-pair exp-6 parameters. However, the uncertainties in these values are about 5%. Moreover, small changes in these parameters can have large effects on the solubility boundary. For example, we can expand the fluid-phase separation region (area under dotted line) far beyond the C-J point simply by changing the r^* parameters for N_2-H_2O and H_2O-CO_2 by +3% and -3.5%, respectively.

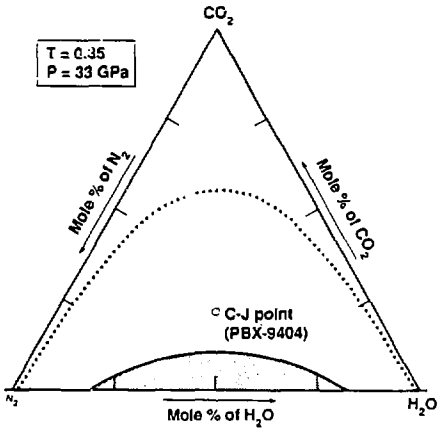

Fig. 9. Theoretical ternary phase diagram (Ref. 37) for the N_2, H_2O, and CO_2 system at 4062 K and 35 GPa that lies close to the theoretical C-J point (open circle) of PBX-9404. See the text for further discusssion.

MULTICOMPONENT SYSTEMS

We briefly describe some multiphase multicomponent applications of the CHEQ code.

Explosives

We assume that the detonation products are in a gaseous mixture and one solid phase, i.e.,

Gas phase A: N_2, H_2O, CO_2, CO, CH_4, NH_3, H_2, O_2, NO
Solid phase: diamond or graphite.

When we tried this procedure for PETN ($C_5H_8N_4O_{12}$) using empirical EOS for the solid products, our calculated C-J point [solid circle in Fig. 10(a)] agreed well with existing experimental data on detonation velocity. When we used the same procedure with PBX-9404 [a plastically bonded composite explosive whose main constituent is HMX ($C_4H_8N_8O_8$)], the lack of agreement was striking [Fig. 10(b)]. For example, at the C-J point [the minimum point in Fig. 10(b)], the theoretical detonation velocity is 9.25 km/s whereas the experimental detonation velocity is 8.78 km/s.

If we compare the computed C-J data for PETN and PBX-9404, we find that, at their respective C-J points, PBX-9404 is cooler than PETN by 540 K but has a higher pressure by 5.4 GPa. This combination of high pressure and low temperature suggested the supercritical phase separation in N_2, H_2O, and CO_2 discussed earlier might affect the detonation behavior, since the three chemical species make up 95% or more of the gaseous detonation products in PBX-9404. Therefore, recalculated the Hugoniot of PBX-9404 taking the possibility of phase separation into account by introducing the second gaseous phase (8):

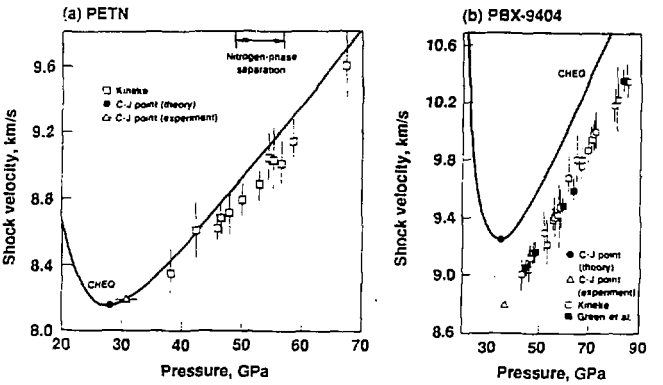

Fig. 10. Shock velocity vs pressure for (a) PETN and (b) PBX-9404, calculated with the CHEQ code and compared with experimental data of Green et al. and Kineke and West. (References on the experimental data are given in Ref. 37.) The calculations assume a single gas phase plus solid carbon.

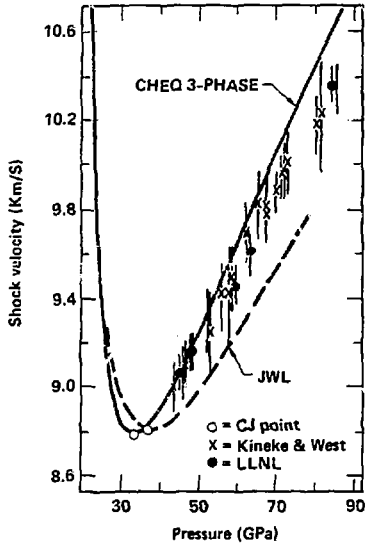

Fig. 11. Shock velocity vs pressure for PBX-9404 (Ref. 37), calculated with the CHEQ code and allowing the possibility of a second gas phase plus solid carbon. (References on the experimental data are given in Ref. 37.)

Gas phase B: N_2, H_2O.

The "three-phase" CHEQ result in Fig. 11 admits phase B only if its presence minimizes the Gibbs free energy. Theory and experiment agree to about 60 GPa. Further experiment would be needed to substantiate this interesting theoretical prediction.

Planetary Interiors

Recently, Nellis et al.[40] have carried out shock pressure measurements on a mixture of H_2O, NH_3, and C_3H_8O (isopropanol). They chose the mole fractions, (H_2O:NH_3:C_3H_8O) = (0.71:0.14:0.15), so that (O:C) and (O:N) ratios match close to those of cosmological abundances, and an (H:O) ratio similar to that of an "ice"-gas mixture in a proposed model of Uranus.[41] High temperatures and pressures created by the shock wave experiment allow the dissociation products from this "synthetic Uranus" to achieve a (P,T) state relevant to an interior point of Uranus. Hence, a theoretical analysis of the shock experiment yields information relevant to the interior composition of Uranus.

Our analysis[40] of the shock experiment with the CHEQ code considers the same species (nine gaseous species and two solids) as in the explosive case. Figure 11 compares two theoretical Hugoniots with the experimental data. The solid and dashed curves correspond, respectively,

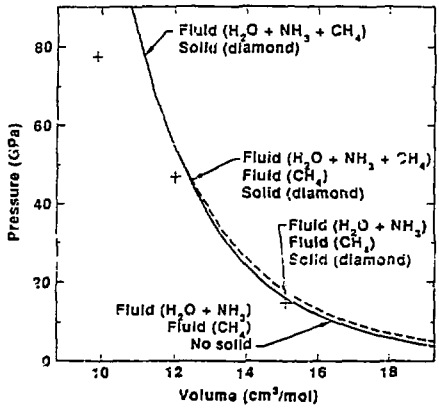

Fig. 12. Hugoniot of synthetic Uranus (Ref. 40). Pluses are experimental data; solid and dash lines represent calculations with and without fluid phase separations, respectively.

to calculations with and without allowing a fluid phase separation. Differences between the two are small, but the case with fluid phase separation agrees better with experiment. At pressures below 20 GPa and shock temperatures near 2000 K, which is relevant to an interior point of Uranus, the calculation suggests that CH_4 molecules prefer to separate out from the (H_2O-NH_3)-rich fluid phase. Since the two coexisting fluid phases have different densities, the gravity of Uranus will segregate the two phases. However, gravity may or may not produce a layered structure (of a type proposed by Hubbard and MacFarlane).[42] At higher shock pressures in Fig. 12, the shock heating reduces the amount of "demixing" of the two fluid phases. At pressures above 50 GPa, the calculation shows no fluid phase separation, and the computed results start to deviate from experiment. The chemical equilibrium calculation does not include monatomic and ionic species, which may occur at high shock pressures and temperatures. Therefore, their omission could explain the observed deviation.

SUMMARY

Both real and computer experiments have produced a large body of thermodynamic data on mixtures at high densities. These data provided an opportunity to construct a high-pressure and high-temperature mixture model. One requirement placed in the mixture model is that it should be applicable not simply to binary systems but also to systems with a large number (≈10) of chemical species. Such a model is needed, for example, to describe the detonation behavior of condensed explosives and the interior structures of the outer planets. Another requirement is that the mixture model uses fundamental theories of statistical mechanics and intermolecular forces.

For this purpose, we adapted the most practical approach, i.e., an "effective" one-component model, which replaces all molecular inter-

actions in the mixture by a hypothetical one-component potential. The best known effective one-component model, i.e., the one-fluid van der Waals (vdWlf) model is not suitable for the present purpose, since it uses the same stiffness α of repulsion for all molecular interactions, an assumption which is not valid at high densities. High-density thermodynamic properties depend sensitively on α's of individual intermolecular repulsions. To circumvent this difficulty, we developed an improved vdWlf model that uses a m'xing formula for α. For mixtures with a light element needing quantum correction, we obtained an analogous effective one-component formula for mass. Monte Carlo simulations on mixture systems were carried out to verify that the improved vdWlf model is as accurate as the conventional vdWlf model but it can be used over an extended density and temperature range where the conventional model is physically inappropriate. Some theoretical justifications for the one-fluid approximations have been described.

The solubility of H_2-He mixtures was chosen as the first application of the mixture model. The theoretical solubility lines are computed by solving for mole fractions at which the Gibbs free energy of the mixtures has a common tangent. The computed results are compared against the diamond anvil cell data to 8 GPa. For the second example, i.e., solubility diagrams of the He-Xe system, we used an alternative but more general approach that is applicable to any multicomponent system. This approach uses a computer code (CHEQ) which solves for the composition of chemical species under the Gibbs equilibrium conditions. The computed results are compared with experimental data. Next we examined supercritical fluid phase separations in mixtures of polar and nonpolar molecules. Here, we approximated an average electrostatic attraction in polar molecules by a temperature-dependent attractive well-depth. Results for N_2-H_2O and CO_2-H_2O mixtures show that the former system exhibits a limited solubility at high pressures and temperatures, but the latter does not. These results are consistent with low pressure experimental data. Next, we considered the supercritical fluid phase separation in a ternary system of N_2, H_2O, and CO_2. We find that CO_2 molecules tend to make N_2 more soluble in water, in much the same way that soap makes oil and water more miscible.

We then shifted our attention to more practical problems involving chemical reactions: the detonation behavior of condensed explosives and a prediction of chemical species at the interior of the giant planets. Experimental data on explosives are available over a wide range of pressures (1-100 GPa) and temperatures (1000-5000 K). We have analyzed PBX-9404 as a typical explosive. The calculation predicts N_2 molecules prefer to separate out from the remaining fluid mixture. Introduction of such a phase separation gives better agreement with experimental shock wave data of PBX-9404. For a planetary application, we used the CHEQ code to interpret a recent Livermore gas-gun experiment of "synthetic" Uranus. In this case, the calculation predicts a fluid-fluid phase separation between a CH_4-rich fluid and a (H_2O-NH_3)-rich fluid at a pressure and temperature condition relevant to an interior point of Uranus.

ACKNOWLEDGMENT

This work was performed under the auspices of the U. S. Department of Energy by Lawrence Livermore National Laboratory under Contract No. W-7405-Eng-48.

REFERENCES

1. (a) L. L. Lee and D. Levesque, Perturbation theory for mixtures of simple liquids, Mole. Phys. 26:1351 (1973); (b) G. Zerah and J.-P. Hansen, Self-consistent integral equations for fluid pair distribution functions: another attempt, J. Chem. Phys. 84:2336 (1986); (c) E. Enciso, F. Lado, M. Lombardero, J. L. F. Abascal, and S. Lago, Extension of the optimized RHNC equation to multicomponent liquids, J. Chem. Phys. 87:2249 (1987).
2. For recent works on shock wave, refer to "Shock Waves in Condensed Matter - 1987," S. C. Schmidt and N. C. Holmes, eds., North-Holland, Amsterdam (1988).
3. Static and dynamic experimental papers by U.S.A., French, and Soviet groups were presented at the XIth AIRPAPT International High Pressure Conference, Kiev, USSR (1987). The conference proceedings will be soon published by Naukova Dumka, Kiev, USSR.
4. (a) L. C. van den Bergh, J. A. Schouten, and N. J. Trappeniers, Fluid-fluid, fluid-solid, and three-phase equilibria in the system helium-hydrogen at pressures to 75 kbar, Physica 141A:524 (1987); (b) P. Loubeyre, R. Le Toullec, and J. P. Pinceaux, Binary phase diagram of H_2-He mixtures at high temperature and high pressure, Phys. Rev. B 36:3723 (1987).
5. M. Ross and F. H. Ree, Repulsive forces of simple molecules and mixtures at high density and temperature, J. Chem. Phys. 73: 6142 (1980).
6. (a) M. S. Shaw, J. D. Johnson, and B. L. Holian, Effective spherical potentials for molecular fluids, Phys. Rev. Lett. 50:1141 (1983); (b) J. L. Lebowitz and J. K. Percus, Sphericalization of nonspherical molecules, J. Chem. Phys. 79:443 (1983).
7. F. H. Ree, Simple mixing rule for mixtures with exp-6 interactions, J. Chem. Phys. 78:409 (1983).
8. F. H. Ree, A statistical mechanical theory of chemically reacting multiphase mixtures: application to the detonation properties of PETN, J. Chem. Phys. 81:1251 (1984).
9. F. H. Ree and C. Bender, Repulsive molecular interactions between two H_2 molecules, J. Chem. Phys. 71:5362 (1979).
10. F. H. Ree and N. W. Winter, Ab initio and Gordon-Kim intermolecular potentials for two nitrogen molecules, J. Chem. Phys. 73:322 (1980).
11. M. Ross, A high-density fluid perturbation theory based on an inverse 12th-power reference system, J. Chem. Phys. 71:1567 (1979).
12. (a) W. J. Nellis, N. C. Holmes, A. C. Mitchell, and M. van Thiel, Phase transition in fluid nitrogen at high densities and temperatures, Phys. Rev. Lett. 51:1661 (1984); (b) H. B. Radousky, W. J. Nellis, M. Ross, D. C. Hamilton, and A. C. Mitchell, Molecular dissociation and shock-induced cooling in fluid nitrogen at high densities and temperatures, Phys. Rev. Lett. 57:2419 (1986).
13. M. Ross, The dissociation of dense liquid nitrogen, J. Chem. Phys. 86:7110 (1987).
14. D. F. Calef and F. H. Ree, Estimate of the barrier to and rate of dissociation of dense nitrogen under shock conditions, Phys. Rev. B 36:4935 (1987).
15. D. C. Hamilton and F. H. Ree, Chemical equilibrium calculations on the molecular-to-nonmolecular transition of shock compressed liquid nitrogen, a preprint.
16. F. H. Ree, Molecular interaction of dense water at high temperature, J. Chem. Phys. 76:6287 (1982).
17. A. C. Mitchell and W. J. Nellis, Equations of state and electrical conductivities of water and ammonia, J. Chem. Phys. 76:6273

(1982).
18. F. H. Ree and C. F. Bender, Nonadditive interaction in molecular hydrogen at high pressure, Phys. Rev. Lett. 32:85 (1974).
19. L. F. Silvera and V. V. Goldman, The isotropic intermolecular potential for H_2 and D_2 in solid and gas phases, J. Chem. Phys. 69:4219 (1978).
20. M. Ross, F. H. Ree, and D. A. Young, The equation of state of molecular hydrogen at high density, J. Chem. Phys. 79:1487 (1983).
21. W. J. Nellis, A. C. Mitchell, and M. van Thiel, Equation-of-state data for molecular hydrogen and deuterium at shock pressures in the range 2-76 GPa (20-760 kbar), J. Chem. Phys. 79:1480 (1983).
22. (a) H. S. Kang, C. S. Lee, T. Ree, and F. H. Ree, A perturbation theory of classical equilibrium fluids, J. Chem. Phys. 82:414 (1985); (b) H. S. Kang, T. Ree, and F. H. Ree, A perturbation theory of classical solids," J. Chem. Phys. 84:4547 (1986).
23. D. Henderson and P. J. Leonard, Liquid mixtures. in: "Physical Chemistry - An Advanced Treatise," D. Henderson, ed., Academic Press, New York (1971).
24. W. R. Smith, Perturbation theory and one-fluid corresponding states theories for fluid mixtures, Can. J. Chem. Eng. 50:271 (1972).
25. D. MacGowan, J. L. Lebowitz, and E. M. Waisman, van der Waals one-fluid theory: justification and generalization, Chem. Phys. Lett. 114:321 (1985).
26. T. W. Leland, Jr. and P. S. Chappelear, the corresponding states principle--a review of current theory and practive, Ind. Eng. Chem. 60:15 (1968).
27. F. H. Ree, Solubility of H_2-He mixtures in fluid phases to 1 GPa, J. Phys. Chem. 87:2846 (1983).
28. J. A. Barker, R. A. Fisher, and R. O. Watts, Liquid argon: Monte Carlo and molecular dynamics calculations, Mol. Phys. 21:657 (1971).
29. W. B. Streett, Phase equilibria in molecular hydrogen-helium mixtures at high pressures, Astrophys. J. 186:1107 (1973).
30. D. A. Young, A. K. McMahan, and M. Ross, Equations of state and melting curve of helium to very high pressure, Phys. Rev. B 24:5119 (1081).
31. T. W. Melnyk and B. L. Sawford, Equation of state of a mixture of hard spheres with nonadditive diameters, Mol. Phys. 29:891 (1975).
32. J. L. Lebowitz and D. Zomick, Mixtures of hard spheres with nonadditive diameters. Some exact results and solution of PY equation, J. Chem. Phys. 54:3335 (1971).
33. B. J. Alder, Studies in molecular dynamics. III. a mixture of hard spheres, J. Chem. Phys. 40:2724 (1964).
34. F. H. Ree, A new approach to multiphase equilibria: application to high-pressure physics problems, Physica B 139 & 140:73 (1986).
35. J. de Swaan Arons and G. A. M. Diepen, Gas-gas equilibria, J. Chem. Phys. 44:2322 (1966).
36. M. J. Hiza and A. G. Duncan, A correlation for the prediction of interaction energy parameters for mixtures of small molecules, AIChE J. 16:733.
37. F. H. Ree, J. Chem. Phys., Supercritical fluid phase separations: implications for detonation properties of condensed explosives, J. Chem. Phys. 84:5845 (1986).
38. (a) V. M. Prokhorov and D. S. Tsiklis, Gas-gas equilibrium in nitrogen-water system, Russ. J. Phys. Chem. 44:1173 (1980); (b) M. L. Japas and E. U. Franck, High pressure phase equilibria and PVT-data of the water-nitorgen system to 673 K and 250 MPa, Ber. Bunsenges. Phys. Chem. 89:793 (1985).
39. K. Tödheide and E. U. Franck, Das Zweiphasengebiet und die kritische Kurve im System Kohlendioxid-Wasser bis zu Drucken von 3500 bar, Z. Phys. Chem. Naue Folge 37:387 (1963).

40. W. J. Nellis, D. C. Hamilton, N. C., Holmes, H. B. Radousky, F. H. Ree, A. C. Mitchell, and M. Nicol, The nature of the interior of Uranus based on studies of planetary ices at high dynamic pressure, Science (1988), (submitted).
41. R. L. Kirk and D. J. Stevenson, Hydromagnetic constraints on deep zonal flow in the giant planets, Astrophys. J. 316:836 (1987).
42. W. B. Hubbard and J. M. MacFarlane, Structure and evolution of Uranus and Neptune, J. Geophys. Res. 85:225 (1980).